Neuron
Article

Synaptic Vesicles Position Complexin to Block Spontaneous Fusion

Rachel T. Wragg,[1] David Snead,[1,3] Yongming Dong,[2,3] Trudy F. Ramlall,[1] Indu Menon,[1] Jihong Bai,[2] David Eliezer,[1] and Jeremy S. Dittman[1,*]
[1]Department of Biochemistry, Weill Cornell Medical College, 1300 York Avenue, New York, NY 10065, USA
[2]Division of Basic Sciences, Fred Hutchinson Cancer Research Center, 1100 Fairview Avenue N, A2-185, Seattle, WA 98109, USA
[3]These authors contributed equally to this work
*Correspondence: jed2019@med.cornell.edu
http://dx.doi.org/10.1016/j.neuron.2012.11.005

SUMMARY

Synapses continually replenish their synaptic vesicle (SV) pools while suppressing spontaneous fusion events, thus maintaining a high dynamic range in response to physiological stimuli. The presynaptic protein complexin can both promote and inhibit fusion through interactions between its α-helical domain and the SNARE complex. In addition, complexin's C-terminal half is required for the inhibition of spontaneous fusion in worm, fly, and mouse, although the molecular mechanism remains unexplained. We show here that complexin's C-terminal domain binds lipids through a novel protein motif, permitting complexin to inhibit spontaneous exocytosis in vivo by targeting complexin to SVs. We propose that the SV pool serves as a platform to sequester and position complexin where it can intercept the rapidly assembling SNAREs and control the rate of spontaneous fusion.

INTRODUCTION

Regulated neurotransmitter release is essential to nervous system function. The presynaptic terminal continually replenishes a pool of synaptic vesicles (SVs) which are docked at the plasma membrane and primed to undergo fusion upon calcium entry. SVs also occasionally fuse with the plasma membrane in the absence of calcium influx, creating an unregulated basal level of secretion. This spontaneous fusion rate must be maintained at a relatively low level to prevent depletion of the SV pool and to maximize the dynamic range of the synapse by minimizing noise levels. The key proteins controlling SV fusion are the neuronal SNARE proteins syntaxin 1, SNAP-25, and VAMP2/synaptobrevin 2, as well as a core set of SNARE-binding proteins including synaptotagmin, Munc13, Munc18, tomosyn, and complexin (Ashery et al., 2009; Brose, 2008; Jahn and Fasshauer, 2012; Kasai et al., 2012; Südhof and Rizo, 2011). Of these proteins, complexin plays a major role in preventing high rates of spontaneous fusion (Cho et al., 2010; Hobson et al., 2011; Huntwork and Littleton, 2007; Kaeser-Woo et al., 2012; Martin et al., 2011; Maximov et al., 2009), and loss of complexin reduces the SV pool by 50% in *C. elegans* (Hobson et al., 2011). Consistent with this inhibitory function, complexin also decreases SNARE-mediated proteoliposome fusion in vitro (Chicka and Chapman, 2009; Schaub et al., 2006). At several mammalian synapses, loss of complexin does not result in an increase in spontaneous fusion, indicating that its inhibitory function can be modulated or perhaps replaced by other synaptic proteins (Strenzke et al., 2009; Xue et al., 2008). Differences in complexin roles at distinct synapses highlight a need for better mechanistic understanding of its function.

Complexin is a cytoplasmic protein comprised of a highly charged α-helical domain subdivided into the accessory helix (residues 23–47) and the central helix (residues 48–70), flanked by N- and C-terminal unstructured regions (Bracher et al., 2002; Chen et al., 2002). The central helix binds the SNARE complex in the groove formed by synaptobrevin 2 and syntaxin 1 and is essential for all known complexin functions, whereas the C-terminal half (residues 71–134) was previously believed to be dispensable (Xue et al., 2007). In *C. elegans* (Martin et al., 2011), *Drosophila* (Cho et al., 2010; Xue et al., 2009), and mouse (Kaeser-Woo et al., 2012), complexin's C-terminal domain (CTD) has been implicated in the inhibition of spontaneous SV fusion even though no direct mechanism has been proposed for its inhibitory function. Biochemical studies of the mammalian complexin 1 isoform found that the CTD interacts with phospholipids via a small amphipathic region near the C terminus, suggesting a role for membrane interactions in complexin function (Seiler et al., 2009). Furthermore, some complexin isoforms associate with membranes via a prenylated CAAX motif at their C termini, and mutating the CAAX box prevented complexin from inhibiting spontaneous fusion (Cho et al., 2010; Xue et al., 2009), indicating membrane binding may be required for this function.

Precise registration of SNARE and complexin residues is required for complexin's inhibitory mechanism, involving conformations that may occur inefficiently in solution (Krishnakumar et al., 2011; Kümmel et al., 2011). How is complexin positioned to engage the assembling SNARE complex? Is the SNARE-clamping function of complexin accelerated by its membrane interactions? Does complexin interact specifically with SV membranes or with the plasma membrane? Using a combination of biochemical, genetic, electrophysiological, and imaging approaches in *C. elegans*, we found that worm complexin, CPX-1, possesses a conserved amphipathic region near its C terminus that is required for suppression of neurotransmitter secretion.

This region interacts with phospholipid bilayers and localizes CPX-1 to SVs where it can rapidly cycle on and off the membrane. We identified similar amphipathic regions in all available complexin sequences across phylogeny regardless of whether a CAAX motif was present. Thus, we propose that membrane localization of complexin is a requirement for its ability to intercept the assembling SNARE complex and prevent unregulated SV fusion events.

RESULTS

CPX-1 Binds Liposomes through a Conserved C-Terminal Amphipathic Region

In *C. elegans*, CPX-1 modulates synaptic vesicle exocytosis by simultaneously inhibiting spontaneous fusion while promoting fusion triggered by a depolarizing electrical stimulus (Hobson et al., 2011; Martin et al., 2011). These two modes of exocytosis can be experimentally distinguished, as CPX-1 lacking the last 50 amino acids of its CTD can partially rescue enhancement of stimulus-evoked exocytosis, but not inhibition of spontaneous SV fusion (Martin et al., 2011). The complexin CTD regions from worm, fly and mouse contain a relatively well-conserved amphipathic region near the C terminus (Figures 1A and 1B), whereas mammalian complexins 3 and 4, along with many other complexin orthologs, also contain C-terminal CAAX boxes (see Figures S1A and S1B available online). Since the amphipathic region appears to be conserved and to confer lipid binding in mammalian complexins (Seiler et al., 2009), we asked whether the homologous region of worm CPX-1 can interact with liposomes.

To examine potential interactions of the CTD with lipids, recombinant CPX-1::GFP fusion protein was incubated with liposomes and centrifuged in a sucrose gradient. Fractions were recovered from the top of the gradient and examined by SDS PAGE and immunoblotting. Wild-type (WT) CPX-1 comigrated with liposomes in the topmost fractions (Figure 1C), and the interaction did not depend on calcium (data not shown). Insertion of a helix-breaking proline (K123P) into the amphipathic region modestly decreased liposome binding, while deleting the C-terminal 50 residues (ΔCT) or exchanging L117 and V121 with glutamates (LV/EE) largely eliminated the liposome interaction (Figures 1C and 1D). About 13% of CPX-1::GFP cosedimented with liposomes containing anionic phospholipids, consistent with a relatively low-affinity interaction (Figure 1E). Protein concentrations were well below the expected saturation point of liposome binding sites (Experimental Procedures). Liposomes composed entirely of phosphatidylcholine (PC) no longer cosedimented CPX-1 suggesting that liposome association depended in part on interactions with anionic phospholipids. Thus, despite a low overall sequence homology within the CTD, worm and mammalian complexins share a common lipid-binding amphipathic motif near the C terminus.

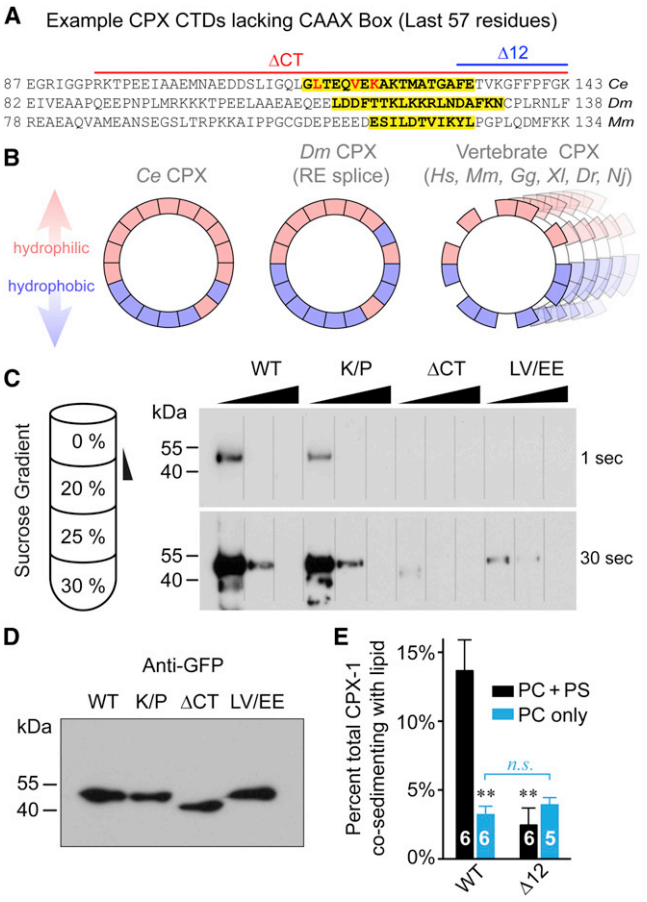

Figure 1. CPX-1 Binds Phospholipids through a Conserved C-Terminal Amphipathic Region

(A) Alignments of the last 57 amino acids from worm (*Ce*), fly splice variant cpx-RE (*Dm*), and mouse (*Mm*) complexin 1 with the amphipathic region highlighted (yellow). ΔCT (*red*) indicates residues 94–143 deleted in the ΔCT CPX-1 construct and Δ12 (blue) indicates residues 132–143 deleted in the Δ12 CPX-1 construct. Substituted residues in this study are indicated in red.

(B) Helical wheel diagrams of the amphipathic region for worm, fly, and six vertebrate complexin 1 orthologs: human (*Hs*), mouse (*Mm*), chicken (*Gg*), *Xenopus* (*Xl*), zebrafish (*Dr*), and skate (*Nj*). Hydrophilic residues are in red, hydrophobic in blue.

(C) Liposome flotation in a sucrose gradient for pGFP-tagged full-length (*WT*), K123P (*K/P*), CTD truncation (*ΔCT*), and L117E, V121E (*LV/EE*). The top three fractions were collected, and floating CPX-1::pGFP was detected by western blot using an anti-GFP antibody. Loading controls displayed on western blot using anti-GFP (D).

(E) Percent cosedimentation of either full-length CPX-1::pGFP or Δ12::pGFP with either 100% phosphatidylcholine (PC) liposomes (blue) or 70% PC + 30% phosphatidylserine (PS) liposomes (black) was quantified across several experiments (see Experimental Procedures and Figure S1). Data are mean ± SEM and ** denotes significantly different from full-length CPX-1 with PC/PS liposomes ($p < 0.01$) using Tukey-Kramer method.

Solution-State NMR Measurements Reveal an Interaction between C-Terminal Residues of CPX-1 and Phospholipids

To further investigate the interaction between CPX-1 and phospholipids, we acquired and compared proton-nitrogen single quantum coherence (HSQC) NMR spectra of full-length CPX-1 in the absence and presence of liposomes (Figure S2A). A subset of resonances exhibited decreased intensity in the presence of liposomes, suggesting a lipid interaction. Regions outside of complexin's central helix are largely disordered, so residues not in direct contact with lipids should retain significant mobility (and therefore high signal intensity) in the presence of liposomes.

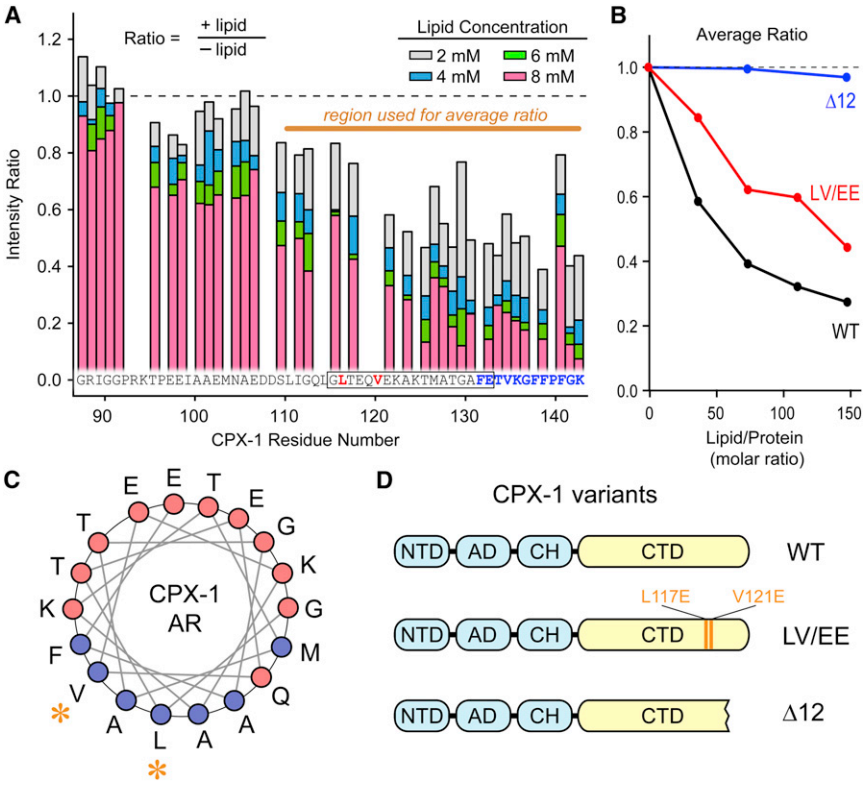

Figure 2. NMR Spectroscopy Reveals an Interaction between Phospholipids and CTD Residues of CPX-1

(A) HSQC peak intensity ratio (with/without lipid) is plotted for each residue of CPX-1 for which a resonance could be well resolved (see Figure S2 for spectrum). Ratios were computed for matched spectra collected at four lipid concentrations as indicated. The amphipathic region is boxed and residues 132–143 deleted in the Δ12 CPX-1 construct are indicated in blue. Substituted residues in this study are indicated in red.

(B) HSQC resonance ratios were averaged over resolvable peaks in the last 34 residues for wild-type full-length CPX-1 (black) and the LV/EE variant (red), or Δ12 (blue) for increasing phospholipid/protein ratio (computed as the molar ratio of total phospholipid to total protein).

(C) Helical wheel model for the amphipathic region with L117 and V121 indicated (asterisks).

(D) Cartoon of the three CPX-1 constructs for which spectra were obtained.

In contrast, residues that interact directly with the phospholipid bilayer will be considerably immobilized, resulting in broad resonance lines and low signal intensity. Figure 2A shows HSQC intensity ratios for well-resolved residues within positions 87–143 of the full-length CPX-1. Complexin residues preceding position 92 were largely unaffected by the presence of liposomes. In contrast, the amphipathic region and neighboring amino acids exhibited a pronounced dose-dependent decrease in signal intensity (Figure 2B). This drop in signal intensity was attenuated when the LV/EE mutation was introduced, consistent with the liposome flotation results above. Interestingly, the final 12 residues of the CTD demonstrated the strongest lipid interaction, suggesting that although the amphipathic region is required for flotation of CPX-1, lipid binding extends beyond the amphipathic region to the final amino acids. This region includes five hydrophobic side chains and two basic residues, and a similar pattern exists in the final 12 residues of other complexins. Deletion of the last 12 amino acids (Δ12) eliminated coflotation (Figures S1C and S1D) and cosedimentation (Figure 1E) with liposomes and almost completely eliminated lipid binding based on HSQC signal (Figure 2B). The amphipathic region and last 12 residues of complexin appear to comprise a novel lipid-binding motif conserved throughout the complexin protein family.

Complexin CTD Lipid Binding Is Required for Inhibitory Complexin Function In Vivo

Guided by the flotation, sedimentation, and NMR results, several CPX-1 CTD variants with altered lipid binding were introduced into *cpx-1* mutant animals to determine whether lipid-binding correlates with complexin function in vivo. Nematodes paralyze when exposed to the cholinesterase inhibitor aldicarb, and increased secretion of acetylcholine accelerates the rate of paralysis (Dittman and Kaplan, 2008; Miller et al., 1996; Nurrish et al., 1999). Reflecting the loss of complexin's clamping function, *cpx-1* mutants rapidly paralyze when exposed to aldicarb (Hobson et al., 2011; Martin et al., 2011). Wild-type aldicarb sensitivity was restored in *cpx-1* mutants expressing full-length CPX-1, while CPX-1 failed to rescue when missing its last 50 residues (*ΔCT*), last 12 residues (*Δ12*), or with the LV/EE substitution (Figures 3A–3C). Failure to rescue complexin's clamping function was due neither to poor expression nor trafficking of CPX since all CPX variants were tagged with GFP, and only transgenic animals expressing comparable levels of synaptic complexin were used in these studies (Figures S3A and S3B). Rescue with the K123P variant of complexin was intermediate, consistent with its mild defect in lipid binding revealed by liposome flotation (Figure 3C).

To examine the effects of perturbing the CTD on the rate of spontaneous fusion, we recorded synaptic activity at the neuromuscular junction (NMJ) in dissected animals in the absence of external calcium. As reported previously, the spontaneous exocytosis rate was considerably elevated in the absence of CPX-1 (Hobson et al., 2011; Martin et al., 2011), and inhibition could not be restored in the absence of the CTD, whereas full-length CPX-1 could fully rescue (Figures 3D–3F). Consistent with the aldicarb sensitivity data, the LV/EE substitution and Δ12 truncation also completely eliminated complexin's clamping function. Thus, complexin's ability to inhibit SV fusion in vivo mirrors its binding to phospholipids in vitro.

CPX-1 Colocalizes with Synaptic Vesicles at the NMJ

As complexin's lipid binding is critical for its function at the synapse, we next explored complexin's synaptic localization at

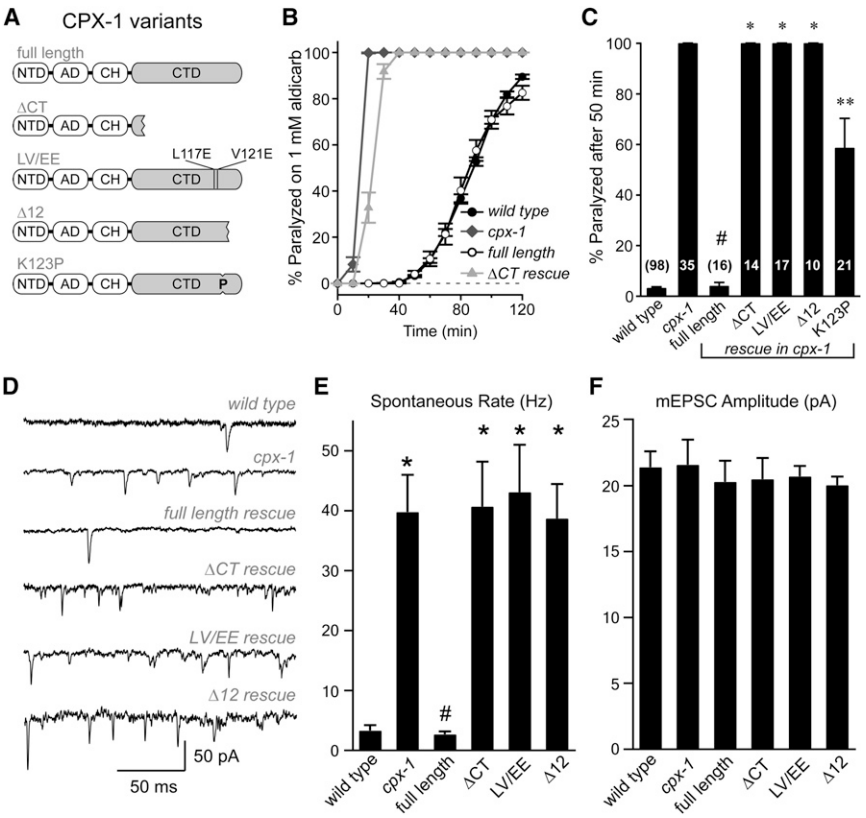

Figure 3. Lipid-Binding Regions of the CTD Are Critical for the Inhibitory Function of CPX-1 In Vivo

(A) Cartoon schematics of the six CPX-1 variants used in these functional studies.

(B) Paralysis time course on 1 mM aldicarb for wild-type (black circles), *cpx-1* (gray diamonds), full-length rescue CPX-GFP (open circles), and a C-terminal truncation ΔCT-GFP (gray triangles).

(C) Percentage of animals paralyzed on 1 mM aldicarb after 50 min for wild-type, *cpx-1* mutant, and transgenic animals expressing CPX-1 variants as indicated.

(D) Examples of spontaneous EPSCs for wild-type, *cpx-1*, and transgenic animals expressing CPX-1 variants as indicated. Average spontaneous (zero external calcium) EPSC Rate (E) and EPSC amplitude (F) for the genotypes indicated in (D).

Data are mean ± SEM and the number of independent assays is indicated for each genotype. * denotes significantly different from wild-type ($p < 0.01$) but not significantly different from *cpx-1*. ** denotes significantly different from both wild-type and *cpx-1*. # denotes no significant difference from wild-type. Significance was determined by the Tukey-Kramer method.

the NMJ. CPX-1::GFP is diffusely distributed throughout motor axons with enrichment at presynaptic terminals (Martin et al., 2011). The synaptic localization of CPX-1::GFP was compared with cytoplasmic mCherry as well as with two canonical synaptic markers: the synaptic vesicle associated RAB-3 and an active zone protein ELKS-1 (Figures 4A–4C). Although complexin appeared to be diffusely distributed throughout the axon, CPX-1::GFP was about 40% more enriched at synaptic boutons than mCherry, indicating that its synaptic enrichment is not merely due to the increased volume of synaptic varicosities. By quantifying the spatial correlation of CPX-1::GFP with either mCherry::RAB-3, soluble mCherry, or ELKS-1::mCherry across a collection of images taken from motor axons of intact animals, CPX-1 appeared to be more robustly colocalized with SVs than with the active zone (Figure 4D). Although the similarity between axonal CPX-1 distribution and SV distribution could imply CPX-1 is associated with SVs, CPX-1 may be bound to the plasma membrane or to SNARE complexes within the bouton, a distinction well beyond the limits of confocal microscopy. To distinguish between these possibilities, CPX-1::GFP was imaged in axons lacking either SVs or the v-SNARE, synaptobrevin. Axonal SVs are largely eliminated in animals harboring a mutation in the anterograde motor *unc-104* KIF1A as a result of impaired vesicle trafficking (Hall and Hedgecock, 1991). Synaptobrevin is mistrafficked in *snb-1(md247)* animals due to a mutation in the transmembrane region (Nonet et al., 1998). While CPX-1::GFP abundance decreased by more than 80% when SVs were eliminated (Figure 4E), there was actually an increase in synaptic CPX-1::GFP when v-SNARE abundance was reduced (Figure 4F). Finally, CPX-1 and RAB-3 were both decreased in an endocytosis mutant (*unc-57* endophilin) while both proteins increased in several exocytosis mutants (*unc-64* syntaxin, *unc-13*, and *unc-18*) (Figure 4G), further supporting the correlation of complexin with vesicle number. Thus, complexin's spatial distribution, insensitivity to SNARE abundance, and strong bidirectional dependence on vesicle number indicate an association with SVs rather than the plasma membrane.

Complexin Is Retained at Presynaptic Boutons Predominantly via Its C-Terminal Domain

Having determined that synaptic CPX-1 localization correlates with the SV pool at the NMJ, we next asked whether the CTD is required for sequestering CPX-1. Steady-state imaging does not report whether CPX-1 is permanently anchored within the synapse or rapidly exchanging between compartments. To measure the residence time of CPX-1 within a synapse, CPX-1 was fused to photoactivatable GFP (pGFP) and expressed in motor neurons along with mCherry::RAB-3 to visualize the SV pool. By photoactivating CPX-pGFP at single synapses in intact animals, the mobility of fluorescent CPX-1 could be monitored and quantified (Figures 5A and 5B). Proteins that are bound to immobile structures within the synapse would be expected to remain within the synapse on a time scale of seconds to minutes, whereas unbound cytosolic proteins should rapidly diffuse out of the synapse and into the adjacent axonal volume. The majority of untagged pGFP diffused out of a synaptic bouton within one second while about half of the CPX-pGFP exhibited a much longer residence time at the synapse, with about 20% remaining after 30 s (Figures 5C–5E). Thus a significant population of

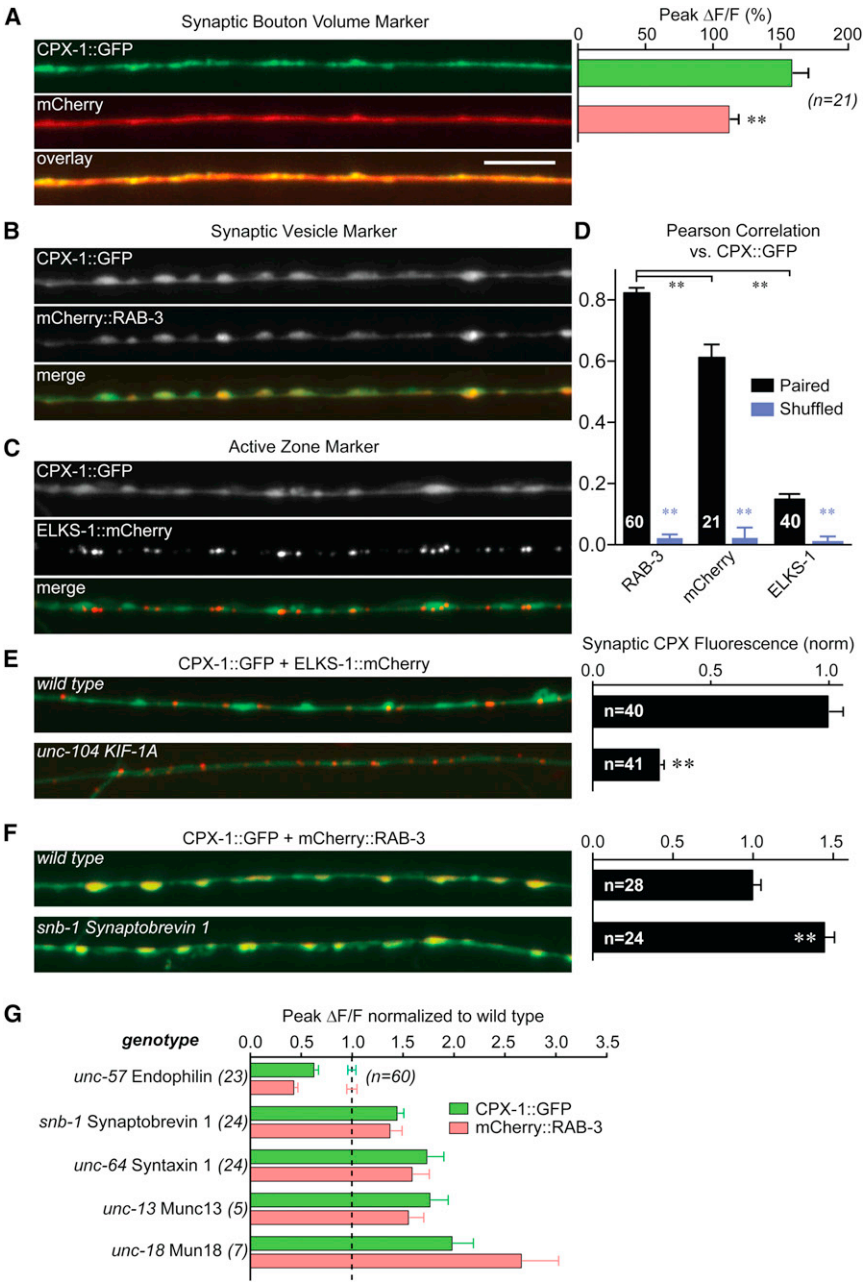

Figure 4. CPX-1 Colocalizes with Synaptic Vesicles at the NMJ

(A) Fluorescent images of the dorsal nerve cord expressing CPX-1::GFP (top), soluble mCherry (middle), and merged image (bottom). Scale bar is 5 μm. Average synaptic enrichment, quantified as $100 \cdot (F_{peak} - F_{axon})/F_{axon}$ for CPX-1::GFP (green) and soluble mCherry (red) is shown on the right.

(B) Fluorescent images of the dorsal nerve cord expressing CPX-1::GFP (top), mCherry::RAB-3 (middle), and merged image (bottom).

(C) Dorsal nerve cord expressing CPX-1::GFP (top), ELKS-1::mCherry (middle), and merged (bottom).

(D) Average Pearson correlation values for pairwise comparisons of CPX-1::GFP fluorescence with mCherry::RAB-3, soluble mCherry, and ELKS-1::mCherry. For each comparison, a shuffled data set was also computed to determine the extent of random correlation between images (see Experimental Procedures).

(E) Dorsal nerve cord expressing CPX-1::GFP and ELKS-1::mCherry in wild-type (top) and *unc-104* KIF-1A mutant (bottom). Average synaptic CPX-1::GFP fluorescence intensity for wild-type and *unc-104* mutants normalized to the wild-type value is shown on the right.

(F) Dorsal nerve cord expressing CPX-1::GFP mCherry::RAB-3 in wild-type (top) and *snb-1* synaptobrevin mutant (bottom). Average synaptic CPX-1::GFP fluorescence intensity for wild-type and *snb-1* mutants normalized to the wild-type value is shown on the right.

(G) Average synaptic enrichment of CPX-1::GFP (green) and mCherry::RAB-3 (red) is shown for *unc-57(e406)* endophilin, *unc-64(e246)* syntaxin 1, *unc-13(s69)*, and *unc-18(e81)* mutants normalized to wild-type (dashed line and error bars for CPX-1::GFP in green, mCherry::RAB-3 in red, n = *60*). Data are mean ± SEM. Number of nerve cord images is indicated in or next to the bar for each measurement.

** denotes significant difference with $p < 0.01$ using the Tukey-Kramer method in (D), or Student's t test in (A), (E), and (F).

CPX-pGFP does not behave like a freely diffusing protein within the synapse, consistent with the steady-state comparisons to soluble mCherry.

Using complexin's long synaptic dwell time as an indication of an interaction at the synapse, we investigated whether the SNARE binding central helix (CH) or the lipid binding CTD influence the kinetics of CPX-pGFP exchange. Deletion of either complexin domain increased mobility, but the CTD played a more significant role in synaptic retention with CPX(ΔCT)-pGFP indistinguishable from pGFP alone by 30 s after photoactivation (Figures 5C–5E). The mobility of the CPX-pGFP variants did not correlate with their synaptic abundance (Figure S3C). Since the only known high-affinity binding partner of complexin is the ternary SNARE bundle, abolishing the ability of complexin to bind synaptic SNARE bundles might be expected to decrease the dwell time of synaptic complexin. However, these experiments show that the CTD is more important in sequestering a pool of synaptic complexin consistent with the localization results described above. The low affinity lipid binding conferred by the CTD provides a simple explanation for synaptic localization of complexin, perhaps reversibly trapping complexin on SVs where it can engage the SNARE proteins.

Tethering CPX-1 to the Plasma Membrane Impairs Its Inhibitory Function

The imaging, biochemistry, and physiology results presented above indicate that complexin is recruited to SVs to engage

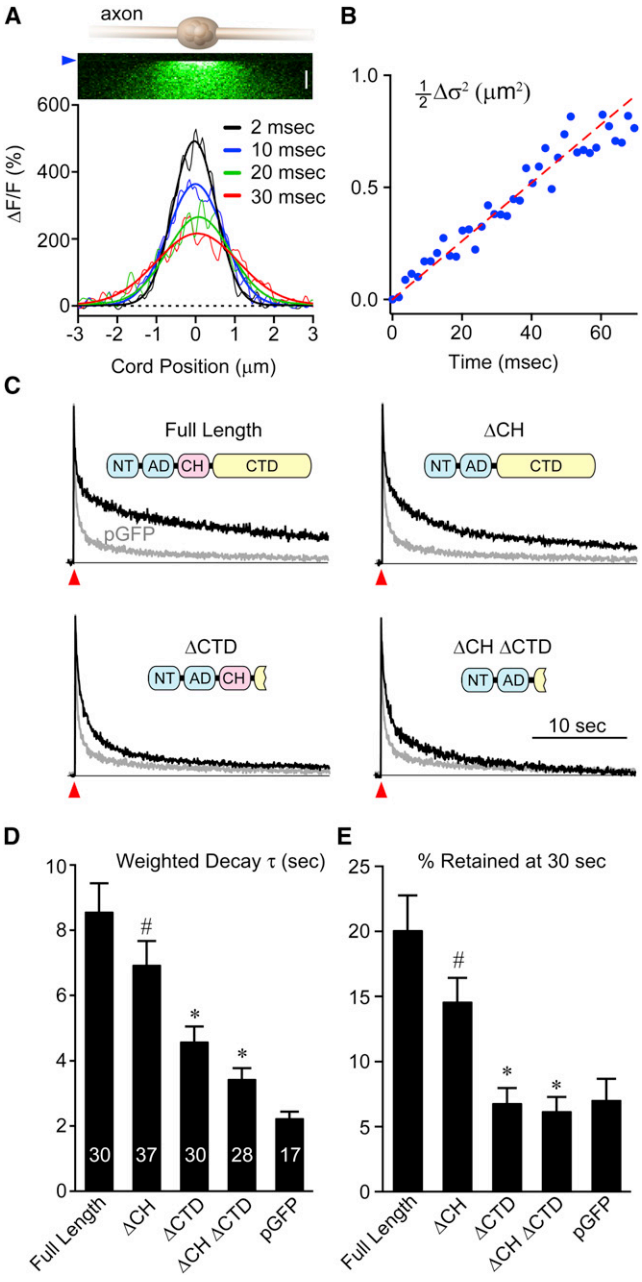

Figure 5. CPX-1 Is Retained at Synapses Primarily through Its CTD

(A) Kymograph of successive line scans following photoactivation of CPX-pGFP (arrowhead) at a single synapse (single trial). Scale bar is 10 ms. Profiles of individual line scans collected after photoactivation at the times indicated (thin traces) were fitted with Gaussians (thick traces).

(B) Increase in variance of fit is plotted versus time and fitted to a line (red) to estimate diffusion (see Experimental Procedures).

(C) Normalized time course of synaptic fluorescence is shown for four CPX-1 variants (black) along with pGFP alone (gray) for comparison. Cartoons of the CPX-1 variants are included for each example time course with protein domains NT (N-terminal domain), AD (accessory domain), CH (central helix), and CTD (C-terminal domain). Activation of pGFP is indicated by the arrowhead.

(D) The weighted decay time constant following a double exponential fit (see Experimental Procedures) is shown for each of the five pGFP constructs.

(E) The percent fluorescence remaining after 30 s. Data are mean ± SEM with number of synapses indicated within bars. * denotes significantly different from full-length ($p < 0.01$) but not significantly different from pGFP. # denotes no significant difference from full-length. Significance was determined by Tukey-Kramer method.

the SNARE bundle and block spontaneous fusion. Is complexin active or inactive when bound to the SV? Could the SV pool serve as a reservoir of inactive complexin, or does complexin require SV interactions in order to function as a clamp?

To address these questions, CPX-1 was targeted either to the plasma membrane or the SV pool using proteins known to be strongly enriched either on the synaptic PM or SVs as artificial anchors. Three anchors were selected to target CPX-1 to the plasma membrane (Figure 6A). K-ras localizes predominantly to the plasma membrane and is anchored by a C-terminal poly-basic stretch and farnesylation of its CAAX box (Hancock, 2003; Willumsen et al., 1984; Zhang and Casey, 1996). The last 23 residues of *let-60* K-ras were attached to full-length CPX-1 to create a plasma-membrane targeted complexin (CPX_{CAAX}). Despite targeting sufficient protein levels within the synapse (Figures 6B and S4A), CPX_{CAAX} could only partially rescue the aldicarb hypersensitivity of *cpx-1* mutants (Figure 6D). If membrane association was disrupted by replacing the terminal cysteine with serine, CPX-1 function could be largely restored (Figures S4B and S4C), demonstrating that anchoring CPX-1 to the plasma membrane interferes with its inhibitory function. Similar results were found when CPX-1 was targeted to the plasma membrane using *unc-64* syntaxin 1A and the PDZ/C2 fragment of *unc-10* RIM1 (Figure 6D). We cannot rule out the possibility that some of the CAAX box or TMR-anchored CPX-1 localizes to SVs as low levels of K-ras and other CAAX box small GTPases have been copurified with SVs (Takamori et al., 2006), and a small percentage of total synaptic syntaxin is found on vesicles (Mitchell and Ryan, 2004; Walch-Solimena et al., 1995). This residual vesicle binding may account for the partial rescue we observed in the plasma-membrane anchored complexins. Taken together, these experiments suggest that tethering full-length complexin to the plasma membrane disrupts its ability to inhibit neurotransmitter release.

CPX-1 Targeted to SVs Is Fully Functional

Full-length CPX-1::GFP was fused to full-length RAB-3 to create a chimeric complexin CPX(SV) specifically targeted to SVs based on the known SV enrichment of this Rab (Schlüter et al., 2002). CPX(SV) localization was indistinguishable from RAB-3 based on confocal imaging and fully restored aldicarb sensitivity in *cpx-1* mutants, in contrast to the plasma membrane anchor chimeras (Figures 6C and 6D). Furthermore, CPX(SV) restored wild-type locomotory behavior whereas CPX(CAAX) was not functional (Figure 6E). Thus, in two independent behavioral assays, SV-targeted CPX-1 fully restored the function of endogenous complexin whereas plasma membrane-associated CPX-1 was not sufficient. Finally, muscle patch-clamp recordings in wild-type, *cpx-1*, and *cpx-1* mutants expressing CPX(SV) demonstrated that SV-targeted CPX-1 could suppress spontaneous fusion with the same efficacy as endogenous CPX-1 (Figures 6F–6H). These experiments indicate that full-length

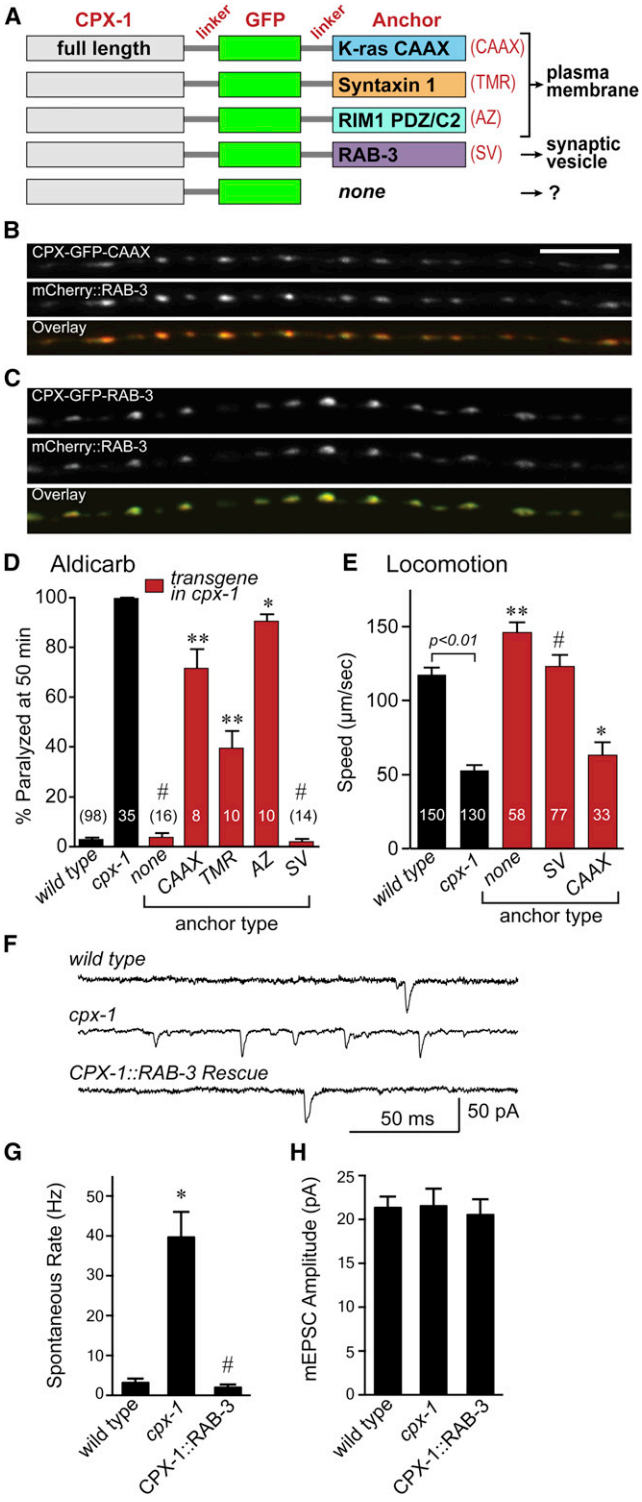

Figure 6. CPX-1 Functions Optimally When Anchored to the Vesicle Rather Than the Plasma Membrane

(A) Schematic of four anchored full-length CPX-1 constructs expressed in *cpx-1* mutants. K-ras CAAX = last 23 residues of worm *let-60* K-ras. Syntaxin 1 = full-length *unc-64* Syntaxin 1. RIM1 PDZ/C2 = 500 amino acid fragment of *unc-10* RIM1. RAB-3 = full-length *rab-3*.

(B) Dorsal nerve cord expressing CPX_{CAAX} and mCherry::RAB-3. Scale bar is 5 µm.

(C) Dorsal nerve cord expressing CPX_{SV} and mCherry::RAB-3.

(D) Percentage of animals paralyzed at 50 min on 1 mM aldicarb for wild-type, *cpx-1*, and five rescue transgenic animals expressing CPX-1 with various anchors as indicated.

(E) Average speed for wild-type, *cpx-1*, and rescue transgenic animals with anchored CPX-1.

(F) Example spontaneous fusion events (at zero external calcium) for wild-type, *cpx-1*, and *cpx-1* mutants rescued with RAB-3-anchored CPX-1.

Average fusion rates (G) and mEPSC amplitudes (H) for the three genotypes in (F). Data are mean ± SEM with number of experiments for aldicarb and number of animals for locomotion indicated. * denotes significantly different from wild-type ($p < 0.01$) but not significantly different from *cpx-1*. ** denotes significantly different from both wild-type and *cpx-1*. # denotes no significant difference from wild-type. Significance was determined by Tukey-Kramer method. Wild-type, *cpx-1*, and full-length rescue aldicarb and electrophysiological data are the same data set shown in Figure 3.

complexin is more effective at clamping the SNAREs when tethered to the SV than when targeted to the plasma membrane.

Complexin's CTD Predominantly Functions to Tether CPX-1 to Synaptic Vesicles

To test the hypothesis that complexin's CTD functions chiefly to anchor complexin to SVs, the ΔCT variant of CPX-1 was targeted to SVs using RAB-3 and to the plasma membrane using the *let-60* K-ras C terminus (Figure 7A). Complexin lacking its CTD failed to suppress elevated ACh levels in the absence of endogenous complexin (Martin et al., 2011). However, when the ΔCT variant was fused to RAB-3 (ΔCT-SV), the majority of complexin's inhibitory function was restored (Figure 7B). Targeting the LV/EE variant to SVs (LV/EE-SV) could also restore the majority of its function in vivo (Figure 7C). In contrast, fusion of the ΔCT variant to the K-ras CAAX domain (ΔCT-CAAX), a plasma membrane-targeted protein, could not replace complexin function (Figures 7B and 7C). It is possible that the CTD participates in other processes beyond tethering complexin to SVs because neither ΔCT-SV nor LV/EE-SV could fully restore CPX-1 function. Nevertheless, much of complexin's inhibitory function could be restored solely by targeting the N-terminal half of complexin to SVs. This highlights a critical role for the lipid-binding CTD in the fusion clamp activity of complexin: steering the SNARE-binding region of complexin onto SVs is required for efficient clamping and prevention of spontaneous fusion.

DISCUSSION

The synapse must maintain tight control over the rate of spontaneous exocytosis to sustain a pool of SVs while minimizing basal noise levels, with complexin functioning as the predominant inhibitor at many synapses. The question of how complexin is directed to the assembling SNARE bundle has not previously been addressed. Several results drawn from our in vitro and in vivo experiments revealed that a region near the end of complexin's CTD interacts with SVs to regulate spontaneous fusion. First, a conserved amphipathic region near the C terminus bound phospholipids as measured by liposome flotation, sedimentation, and NMR spectroscopy. Second, a novel region of complexin's C terminus consisting of the final 12 residues interacted

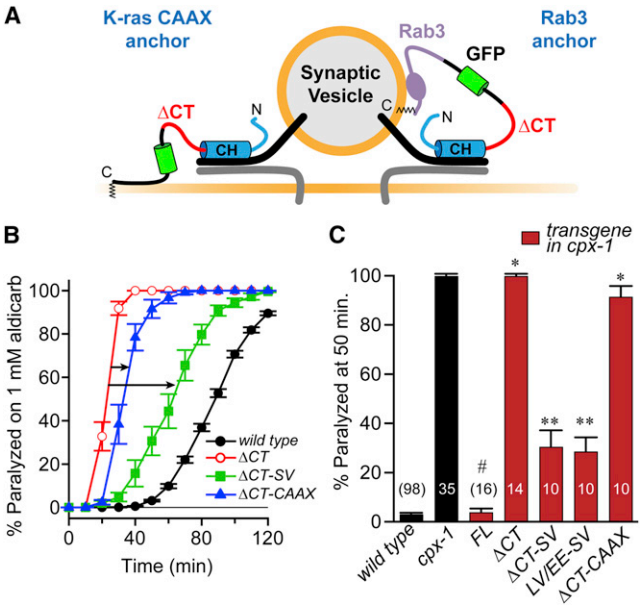

Figure 7. SV Tethering Bypasses the Requirement for the CTD

(A) Cartoon of two rescue constructs expressed in *cpx-1* mutants interacting with the *trans*-SNARE and membrane. In both constructs, the last 50 residues of the CTD have been removed and the remaining N-terminal half of CPX-1 has been fused to GFP and a membrane anchor. The CAAX anchor (left) and SV anchor (right) are described in Figure 6. CH is the central helix.

(B) Time course of paralysis in 1 mM aldicarb for wild-type animals (black) and three transgenic strains expressing the following CPX-1 variants: ΔCT (red circles), ΔCT-SV (green squares), and ΔCT-CAAX (blue triangles).

(C) Percentage paralysis at 50 min for the transgenics shown in (B) as well as *cpx-1*, full-length rescue (*FL*), and the amphipathic mutation LV/EE fused to RAB-3 (*LV/EE-SV*). Data are mean ± SEM with number of experiments for aldicarb indicated on the bar graph.

** Denotes significantly different from *cpx-1* and wild-type ($p < 0.01$). * denotes significantly different from wild-type ($p < 0.01$) but not significantly different from *cpx-1*. # denotes no significant difference from wild-type. Significance was determined by Tukey-Kramer method. Wild-type, *cpx-1*, and full-length rescue aldicarb and electrophysiological data are the same data set shown in Figure 3.

with liposomes. Third, mutations that disrupt lipid binding also prevented complexin from inhibiting neurotransmitter secretion in vivo. Fourth, complexin was sequestered at the synapse primarily through its CTD and colocalized with SVs. And lastly, tethering complexin to SVs bypassed the requirement for the CTD whereas plasma membrane targeting prevented complexin from fully functioning. Since other SNARE-binding proteins such as synaptotagmin and tomosyn are thought to engage the SNARE complex from the SV (McEwen et al., 2006; Takamori et al., 2006; Wang et al., 2011), this dependence on localization and enrichment may be a general feature of proteins tasked with binding a highly dynamic SNARE complex in the act of assembly.

The SV Pool as a Reservoir for Complexin

The SV pool has been proposed to serve as a scaffold capable of buffering synaptic proteins, and complexin was identified as a highly abundant protein enriched within the bouton (Denker et al., 2011). A comprehensive SV protein study found no copurification of complexin with SVs, consistent with a transient, low-affinity SV interaction (Takamori et al., 2006). Our binding and dynamic imaging data suggest that complexin has a low-affinity interaction with liposomes in vitro and SVs in vivo. Since complexin is one of the more abundant proteins at the synapse (Denker et al., 2011), complexin likely saturates the available vesicle binding sites at the synapse and is rapidly exchanging between vesicle surface and the cytoplasm. Even if, as our biochemical and imaging results suggest, complexin's affinity for SVs is low, a cluster of hundreds of closely packed SVs at the synapse would provide the avidity to trap and buffer complexin, maintaining the total abundance at a higher concentration than axonal complexin. Our data do not exclude the possibility that complexin also interacts with other membranes at the synapse, but the artificial tether experiments indicate that complexin's inhibitory function originates from the SV. Further studies will determine whether a specific interaction such as preference for highly curved membrane, particular phospholipids, or binding to SV proteins directs complexin to the SV pool. Thus, the data presented here provide direct mechanistic evidence for the vesicle pool as a platform for the capture and local organization of a key synaptic protein.

Mechanistic Role for the CTD in Aiding Inhibition of SNARE Assembly

In both worm and fly, the spontaneous fusion rate was ten times higher in NMJs lacking complexin, (Hobson et al., 2011; Huntwork and Littleton, 2007; Martin et al., 2011), highlighting complexin's major role in suppressing exocytosis in the absence of stimulation. In addition, overexpression of the ΔCT variant, which does not bind SVs, failed to rescue complexin's inhibitory function in worm, fly, and mouse, suggesting that simply providing a high cytoplasmic concentration may not be sufficient to trap the assembling SNARE bundle effectively (Cho et al., 2010; Kaeser-Woo et al., 2012; Martin et al., 2011; Xue et al., 2009). Why might vesicle-anchored complexin be more effective at stopping SNARE assembly? Complexin is thought to inhibit SV fusion by binding to the partially zippered SNARE complex through its central helix and accessory domain (Giraudo et al., 2009; Kümmel et al., 2011; Maximov et al., 2009; Xue et al., 2007). The central helix sits in the groove formed by syntaxin 1 and synaptobrevin 2 while the accessory domain can interact with a neighboring partially-assembled SNARE bundle situated antiparallel to the first SNARE bundle, in a "zigzag" array conformation (Krishnakumar et al., 2011; Kümmel et al., 2011). Thus, an otherwise rapidly assembling *trans*-SNARE complex requires complexin to engage several sites on multiple polypeptide chains simultaneously. This clamping mechanism will not occur efficiently if complexin is limited by its diffusion from the cytoplasm directly onto the SNARE complex. However, if complexin levels are locally elevated near the SV membrane through low-affinity vesicle binding, the protein could be positioned to catalyze a significantly more rapid and reliable blockade of SNARE assembly. This sort of proximity-accelerated reaction has been observed in other systems where interfacial catalysis occurs, such as enzymes which act on phospholipids (Ramirez and Jain, 1991).

Since complexin binding to the *trans*-SNARE blocks spontaneous fusion, both the abundance and local position of complexin have a direct effect on spontaneous fusion rates. A highly simplified conceptual model of this relationship is depicted in Figure S5. In this model, complexin binds to the pre-fusion SNARE complex prior to full SNARE assembly to reduce spontaneous fusion. Locally elevating and orienting complexin through interactions with the SV will increase the effective rate of binding to the SNARE complex, thereby reducing the rate of spontaneous fusion. Complexin function was impaired when tethered to the plasma membrane, so we propose that intercepting the assembling SNARE complex requires complexin to act from a specific location on the vesicle. Simply creating a high local concentration of complexin on the plasma membrane does not restore blockade of spontaneous fusion. Further exploration of complexin interactions with the SV will be needed to describe the positional requirements of complexin in the act of binding the assembling SNARE complex.

Prenylated Complexins at the Synapse

Several complexin sequences contain CAAX box motifs and the biological significance of prenylation has been demonstrated in both *Drosophila* DmCpx1 and mouse mCpx3 (Cho et al., 2010; Reim et al., 2005), suggesting complexin is specifically targeted to a membrane-associated compartment in some synapses. In fly, at least one splice variant of DmCpx1 must be farnesylated to block spontaneous SV fusion at the larval NMJ (Cho et al., 2010; Xue et al., 2009). Another splice variant of DmCpx1 eliminates the CAAX box but preserves the amphipathic region (Figure 1A), suggesting the possibility that fly complexin splice variants may be differentially targeted, perhaps within distinct neuronal subtypes. Mouse complexin isoforms mCpx3 and 4 are farnesylated and targeted to ribbon synapses of the retina (Landgraf et al., 2012; Reim et al., 2009; Reim et al., 2005). However, the specific effects on SV fusion at these synapses when farnesylated complexins are removed or altered are not yet known. Interestingly, forcing either worm CPX-1 or mCpx1 to be prenylated impairs its inhibitory function in the worm NMJ and mouse hippocampal cultures, respectively (Kaeser-Woo et al., 2012; Figure 6). Perhaps the C-terminal sequences of CAAX-containing complexins target them to synaptic specializations such as the ribbon in photoreceptor terminals, or the T-bar in the fly larval NMJ (Prescott and Zenisek, 2005; Wichmann and Sigrist, 2010), while conventional synapse complexins target SVs directly.

Additional Roles of Complexin at the Synapse

In both worm and mouse, the facilitatory role of complexin during stimulus-evoked synaptic transmission can be partially restored without its CTD (Kaeser-Woo et al., 2012; Martin et al., 2011). Moreover, complexin promotes stimulus-evoked fusion even when tight SNARE binding is disrupted, despite complete elimination of its clamping function (Martin et al., 2011). If neither SV interactions nor tight SNARE binding are required to promote calcium-triggered exocytosis, then how does complexin facilitate this process? Perhaps interactions with other critical synaptic proteins such as synaptotagmin in the context of elevated cytoplasmic calcium can account for this separate functionality of complexin. Further studies will be required to determine the details of these interactions, but the results presented here offer a key mechanistic insight into complexin's inhibitory function, and establish a general mechanism for controlling the abundance and positioning of synaptic proteins guided by low-affinity interactions with the SV pool.

EXPERIMENTAL PROCEDURES

Aldicarb Sensitivity Assays

To measure aldicarb sensitivity, 20–25 young adult animals were placed on agar plates containing 1 mM aldicarb (Chem Services). Worms were scored for paralysis at ten minute intervals for 2 hr. Each genotype was tested at least ten times and paralysis curves were generated by averaging paralysis time courses for each plate as described previously (Dittman and Kaplan, 2008).

Worm Tracking and Analysis

Young adult animals were picked to 6 cm agar plates with no bacterial lawn (40 worms per plate). Imaging began 1 hr after worms were transferred. At least 200 animals were assayed for each genotype. One minute digital videos of individual animals were captured on an ORCA-05G CCD camera (Hamamatsu) mounted on an Olympus SZX16 stereomicroscope at 5 Hz using 10× magnification. Plates were lightly tapped before tracking capture. The center of mass was recorded for each animal on each video frame using custom object tracking software in MatLab (Ramot et al., 2008). Fewer than 10% of worms were excluded due to lack of movement for 30 s or longer.

Steady-State Fluorescence Imaging and Quantification

Animals were immobilized using a 30 mg/ml solution of 2,3-butanedione monoxime (J.T Baker) mounted on 2% agarose pads, and imaged on an inverted Olympus microscope (IX81), using a laser scanning confocal imaging system (Olympus Fluoview FV1000 with dual confocal scan heads) and an Olympus PlanApo 60× 1.42 NA objective. Rescuing complexin variants were C terminally tagged with GFP separated by a 12 residue linker (GGSGGSGGSAAA), and synaptic protein levels were estimated by measuring background-subtracted fluorescence within dorsal cord varicosities. Data were analyzed with custom software in IGOR Pro (WaveMetrics, Lake Oswego, OR) (Burbea et al., 2002; Dittman and Kaplan, 2006). A fluorescent slide was imaged daily to monitor the laser stability and the dorsal cord fluorescence was normalized to the slide value. For the spatial correlation experiments shown in Figure 4, individual line scans where computed from maximal intensity projections of image stacks in each color channel. Green (CPX-1) and red (RAB-3 or ELKS-1) line scans from the same animal were cross-correlated to compute the Pearson correlation coefficient in the paired measurement. Since some of the overlapping fluorescence intensity could have arisen due to chance, we also shuffled the green and red line scans so that green-red correlations between animals could be determined (shuffled correlation). In all cases, the shuffled correlation coefficient was nearly zero, confirming that the measured correlation is not due to chance. $\Delta F/F$ calculations in Figure 4, were made as described previously (Dittman and Kaplan, 2006).

Dynamic Fluorescence Imaging and Quantification

Complexin variants were C terminally tagged with photoactivatable GFP (pGFP) separated by a 12 residue linker (GGSGGSGGSAAA) and coexpressed with mCherry::RAB-3 in dorsal cord motor neurons using a modified *unc-129* promoter. pGFP was photoactivated with a 1 ms pulse from a stationary 405 nm laser beam centered on the synapse of interest based on mCherry::RAB-3 fluorescence. Photoactivated fluorescence was initially distributed over the synapse with a full-width half-maximum ranging from 500 to 800 nm. Line scans of length 5 to 10 μm centered on the target synapse were collected every 1.5–2 ms, depending on the line scan length. Kymographs of sequential line scans were assembled and analyzed to generate time courses of fluorescence decay averaged over a 1 μm region centered on the target synapse. For the CPX-pGFP experiments shown in Figure 5C, small regions of interest measuring 10 by 0.2 μm (400 by 8 pixels) centered on the target synapse were collected every 30 to 40 ms, and each image

was collapsed to a line scan using maximal intensity projection. Consecutive projected line scans were then assembled into a kymograph and analyzed as described above. Experiments were rejected if mCherry::RAB-3 fluorescence revealed large drift or movement artifacts. All analysis was performed in Igor using custom written software. The decay time courses reflect a nontrivial combination of diffusion and binding/unbinding kinetics. In the absence of a detailed reaction-diffusion model to account for the details of synapse geometry, diffusion, and membrane binding, we chose to fit the data empirically using a double exponential decay function. For each synapse, weighted decay times constants were obtained by fitting the normalized, background subtracted data with a double exponential function and computing $\tau_w = (A_{fast}\ \tau_{fast} + A_{slow}\ \tau_{slow})/(A_{fast} + A_{slow})$ where A_{fast} and A_{slow} are the fast and slow amplitudes, while τ_{fast} and τ_{slow} are the fast and slow time constants, respectively. These parameters allow for a quantitative comparison of decay kinetics but are not intended to correspond directly to a measure of either diffusion or unbinding kinetics. For untagged pGFP, diffusion out of the synapse could be estimated by fitting each line scan with a Gaussian centered on the target synapse and analyzing the increase in variance of the Gaussian over time using the formula:

$$D_{GFP} = \frac{1}{2}\frac{\left(\sigma^2 - \sigma_O^2\right)}{\Delta t}$$

where σ_o^2 is the initial variance of fluorescence. For simple diffusion, this rate is constant and thus variance will increase linearly with time (see Figure 5B). Using this approach, a moderate range of diffusion constants was observed ranging between 5 and 15 $\mu m^2/s$ at the worm NMJ, consistent with small globular proteins diffusing within a restricted compartment.

Protein Purification

CPX-1(WT)::pGFP (JP249), CPX-1(K/P)::pGFP (JP252), CPX-1(ΔCT)::pGFP (JP253), CPX-1(LV/EE)::pGFP (JP254), and CPX-1(Δ12)::pGFP (JP318) constructs were cloned into the pET28a vector containing a His_6 tag to facilitate purification. These constructs also contain a 34 amino acid sequence at the N-terminus consisting of a T7 tag and thrombin cleavage site. BL21-DE3 *E. coli* were transformed and grown in rich media containing 50 μg/ml kanamycin to an optical density of 0.6. Cells were then induced with 400 μg/ml isopropyl thiogalactopyranoside (IPTG), grown for three hours at 37°C, pelleted, resuspended in buffer (35 mM NaCl, 20 mM imidazole, 20 mM Tris-HCl, 1.5 mM BME, 2 mM DTT), lysed by sonication, and pelleted at 40,000 rpm for 40 min. For NMR samples, cells grown on rich media were spun down and resuspended in a minimal M9 media containing ^{15}N-ammonium chloride with or without ^{13}C-glucose prior to induction. The supernatant was purified on a Ni-NTA column (QIAGEN, Hilden, Germany). Protein was eluted in elution buffer (350 mM NaCl, 250mM Imidazole, 20 mM Tris-HCl, 1.5 mM BME, 2 mM DTT). For assays in Figure 1, concentrated fractions underwent buffer exchange (150 mM NaCl, 50 mM Tris-HCl, 1 mM CaCl, 1 mM DTT) using Sephadex G-25 Fine beads (Sigma). For NMR, pure complexin was dialyzed into 60 mM phosphate, 2 mM DTT, 0.5 mM EDTA, pH 6.1.

Liposome Preparation

Lipids were obtained from Avanti Polar Lipids and stored at −20°C. For anionic liposomes, a lipid mixture composed of 70% 1-palmitoyl-2-oleoyl-phosphatidylcholine (POPC), and 30% 1-palmitoyl-2-oleoyl-phosphatidylserine (POPS) was dried under a stream of N_2 gas, and residual solvent was removed under vacuum for 1 hr. The lipid film was then rehydrated in buffer (150 mM NaCl, 50 mM Tris-HCl, 1 mM $CaCl_2$, 1 mM DTT for flotation, or 60 mM phosphate, 2 mM DTT, 0.5 mM EDTA [pH 6.1] for NMR) to obtain a final lipid concentration of either 4 mM (flotation and co-sedimentation) or 20 mM (NMR). The resulting liposomes underwent 10 cycles of freezing in liquid nitrogen and thawing (50°C water bath), and were then extruded 21 times through either 400 or 200 nm then 100 nm pore-size polycarbonate films using a 10 ml Lipex Extruder from Northern Lipids (Canada) to form unilamellar vesicles.

Liposome Flotation Assay

Protein and lipids were incubated at room temperature for 1 hr. A sucrose gradient (10 mM HEPES, 150 mM NaCl, 1 mM $CaCl_2$) containing 500 μl of the sample mixed with 500 μl 60% sucrose (Amresco), 1 ml 25% sucrose, 1 ml 20% sucrose and 500 μl buffer was constructed. One hundred microliter fractions were obtained after ultracentrifugation in an MLS-50 rotor (Beckman) at 35,000 rpm for 2 hr. Fractions were run on a 10% SDS-PAGE gel followed by western blotting. Protein was detected with a polyclonal rabbit GFP antibody and a horseradish peroxidase conjugated goat anti-rabbit secondary antibody (Genescript) and visualized using chemiluminescence (Thermo Scientific). For the flotation assays, the total amount of protein added was estimated using SDS-PAGE (WT 0.92 μg; K123P 1.2 μg; ΔCT 0.89 μg; LV/EE 0.74 μg for assay shown in Figure 1C, and WT 9.6 μg; Δ12 40.8 μg for the assay shown in Figure S1C) with bands quantified using ImageJ. The protein:liposome ratio for these experiments ranged from 4:1 to 200:1, which is more than an order of magnitude below the expected ratio of binding sites:liposome (~4,400:1, estimated using the surface area occupied by a 30-residue helix freely rotating about its center on the surface of a 150 nm diameter liposome) (Georgieva et al., 2010).

Liposome Cosedimentation Assay

Full-length and Δ12 CPX-1 proteins were spun at 75,000 rpm for 30 min to eliminate potential protein aggregates and then incubated with lipids at room temperature for 1 hr. Twenty microliter fractions were taken from the ~70 μl supernatant and the resuspended pellet after ultracentrifugation in a TLA100.1 rotor (Beckman) at 75,000 rpm for 30 min. The fractions were run on a 10% SDS-PAGE gel and examined using ImageJ. Percent cosedimentation was calculated as 100 × P/(P + 3.5 × S), where P is the pellet band intensity and S is the supernatant band intensity. The cosedimentation was performed six times, and the calculated cosedimentation percentage was averaged. Protein:liposome ratios were about 20:1 for these assays.

NMR Spectroscopy

Proton-nitrogen correlation (HSQC) spectra as well as a standard set of heteronuclear triple resonance three-dimensional spectra (HNCACB/CBCACONH, HNCACO/HNCO, and HNCANH) were collected on either a Varian Unity Inova 600 MHz (Weill Cornell NMR Facility) or a Bruker AVANCE 700 MHz (New York Structural Biology Center) spectrometer equipped with a cryoprobe. Backbone resonance assignments for free wild-type complexin were obtained at a completeness level of 91% for amide group, Cα, and Cβ, and 87% for CO resonances, except for the N-terminal tag region and residues 40–66, the latter of which were not assigned due to reduced signal intensity and severe overlap, likely originating from the known helical conformation of this region (Chen et al., 2002). Liposome titrations were monitored using HSQC spectra using 1024 and 2564 complex data points in the direct and indirect dimensions, respectively and spectral widths of 12,000 Hz (proton) and 1,600 Hz (nitrogen). All spectra were collected at 20°C with subsaturating protein:liposome ratios. Data were processed using NMRpipe and analyzed using NMRview (Delaglio et al., 1995; Johnson and Blevins, 1994). Spectra were referenced indirectly to water. Protein concentrations were between 50 and 75 μM, as measured using absorbance at 280 nm and an experimentally determined extinction coefficient of 1882 $cm^{-1}M^{-1}$.

Electrophysiology

Whole-cell patch-clamp recordings were performed on dissected animals as described previously (Madison et al., 2005; McEwen et al., 2006). Dissected worms were superfused in an extracellular solution containing 127 mM NaCl, 5 mM KCl, 26 mM $NaHCO_3$, 1.25 mM NaH_2PO_4, 20 mM glucose, 5 mM $MgCl_2$ at 20°C. Whole-cell recordings were carried out at −60 mV using an internal solution containing 105 mM CH_3O_3SCs, 10 mM CsCl, 15 mM CsF, 4 mM $MgCl_2$, 5 mM EGTA, 0.25 mM $CaCl_2$, 10 mM HEPES, and 4 mM Na_2ATP, adjusted to pH 7.2 using CsOH. Under these conditions, we only observed cholinergic EPSCs.

Statistical Analysis

For data sets requiring a single pairwise comparison, we used Student's t test to compute significance. For all other comparisons, we used the Tukey-Kramer method for multiple comparisons. This test assumes independent, normal distributions with equal variance. In cases in which sample variance was significantly different, we employed the Newman-Keuls method to test significance. Significance was defined by the criterion $p < 0.01$.

SUPPLEMENTAL INFORMATION

Supplemental Information includes five figures and Supplemental Text and can be found with this article online at http://dx.doi.org/10.1016/j.neuron.2012.11.005.

ACKNOWLEDGMENTS

We thank Tim Ryan, Anant Menon, Josh Kaplan, Daniel Radoff, Richard Komuniecki, and Michael Hoppa for advice and for critically reading the manuscript, as well as the anonymous reviewers for their helpful suggestions. This work was supported by National Institutes of Health grants R01-GM095674 (J.S.D.), R00-MH085039 (J.B.), R37-AG019391 (D.E.), 5R01GM71041(I.M.), MSTP GM07739 (D.S.), a gift from Herbert and Ann Siegel (D.E.), and the Rita Allen Foundation Award 188423 (J.S.D.).

Accepted: November 3, 2012
Published: January 23, 2013

REFERENCES

Ashery, U., Bielopolski, N., Barak, B., and Yizhar, O. (2009). Friends and foes in synaptic transmission: the role of tomosyn in vesicle priming. Trends Neurosci. *32*, 275–282.

Bracher, A., Kadlec, J., Betz, H., and Weissenhorn, W. (2002). X-ray structure of a neuronal complexin-SNARE complex from squid. J. Biol. Chem. *277*, 26517–26523.

Brose, N. (2008). For better or for worse: complexins regulate SNARE function and vesicle fusion. Traffic *9*, 1403–1413.

Burbea, M., Dreier, L., Dittman, J.S., Grunwald, M.E., and Kaplan, J.M. (2002). Ubiquitin and AP180 regulate the abundance of GLR-1 glutamate receptors at postsynaptic elements in *C. elegans*. Neuron *35*, 107–120.

Chen, X., Tomchick, D.R., Kovrigin, E., Araç, D., Machius, M., Südhof, T.C., and Rizo, J. (2002). Three-dimensional structure of the complexin/SNARE complex. Neuron *33*, 397–409.

Chicka, M.C., and Chapman, E.R. (2009). Concurrent binding of complexin and synaptotagmin to liposome-embedded SNARE complexes. Biochemistry *48*, 657–659.

Cho, R.W., Song, Y., and Littleton, J.T. (2010). Comparative analysis of Drosophila and mammalian complexins as fusion clamps and facilitators of neurotransmitter release. Mol. Cell. Neurosci. *45*, 389–397.

Delaglio, F., Grzesiek, S., Vuister, G.W., Zhu, G., Pfeifer, J., and Bax, A. (1995). NMRPipe: a multidimensional spectral processing system based on UNIX pipes. J. Biomol. NMR *6*, 277–293.

Denker, A., Kröhnert, K., Bückers, J., Neher, E., and Rizzoli, S.O. (2011). The reserve pool of synaptic vesicles acts as a buffer for proteins involved in synaptic vesicle recycling. Proc. Natl. Acad. Sci. USA *108*, 17183–17188.

Dittman, J.S., and Kaplan, J.M. (2006). Factors regulating the abundance and localization of synaptobrevin in the plasma membrane. Proc. Natl. Acad. Sci. USA *103*, 11399–11404.

Dittman, J.S., and Kaplan, J.M. (2008). Behavioral impact of neurotransmitter-activated G-protein-coupled receptors: muscarinic and $GABA_B$ receptors regulate *Caenorhabditis elegans* locomotion. J. Neurosci. *28*, 7104–7112.

Georgieva, E.R., Ramlall, T.F., Borbat, P.P., Freed, J.H., and Eliezer, D. (2010). The lipid-binding domain of wild type and mutant alpha-synuclein: compactness and interconversion between the broken and extended helix forms. J. Biol. Chem. *285*, 28261–28274.

Giraudo, C.G., Garcia-Diaz, A., Eng, W.S., Chen, Y., Hendrickson, W.A., Melia, T.J., and Rothman, J.E. (2009). Alternative zippering as an on-off switch for SNARE-mediated fusion. Science *323*, 512–516.

Hall, D.H., and Hedgecock, E.M. (1991). Kinesin-related gene *unc-104* is required for axonal transport of synaptic vesicles in *C. elegans*. Cell *65*, 837–847.

Hancock, J.F. (2003). Ras proteins: different signals from different locations. Nat. Rev. Mol. Cell Biol. *4*, 373–384.

Hobson, R.J., Liu, Q., Watanabe, S., and Jorgensen, E.M. (2011). Complexin maintains vesicles in the primed state in *C. elegans*. Curr. Biol. *21*, 106–113.

Huntwork, S., and Littleton, J.T. (2007). A complexin fusion clamp regulates spontaneous neurotransmitter release and synaptic growth. Nat. Neurosci. *10*, 1235–1237.

Jahn, R., and Fasshauer, D. (2012). Molecular machines governing exocytosis of synaptic vesicles. Nature *490*, 201–207.

Johnson, B.A., and Blevins, R.A. (1994). NMR View: A computer program for the visualization and analysis of NMR data. J. Biomol. NMR *4*, 603–614.

Kaeser-Woo, Y.J., Yang, X., and Südhof, T.C. (2012). C-terminal complexin sequence is selectively required for clamping and priming but not for Ca^{2+} triggering of synaptic exocytosis. J. Neurosci. *32*, 2877–2885.

Kasai, H., Takahashi, N., and Tokumaru, H. (2012). Distinct initial SNARE configurations underlying the diversity of exocytosis. Physiol. Rev. *92*, 1915–1964.

Krishnakumar, S.S., Radoff, D.T., Kümmel, D., Giraudo, C.G., Li, F., Khandan, L., Baguley, S.W., Coleman, J., Reinisch, K.M., Pincet, F., and Rothman, J.E. (2011). A conformational switch in complexin is required for synaptotagmin to trigger synaptic fusion. Nat. Struct. Mol. Biol. *18*, 934–940.

Kümmel, D., Krishnakumar, S.S., Radoff, D.T., Li, F., Giraudo, C.G., Pincet, F., Rothman, J.E., and Reinisch, K.M. (2011). Complexin cross-links prefusion SNAREs into a zigzag array. Nat. Struct. Mol. Biol. *18*, 927–933.

Landgraf, I., Mühlhans, J., Dedek, K., Reim, K., Brandstätter, J.H., and Ammermüller, J. (2012). The absence of Complexin 3 and Complexin 4 differentially impacts the ON and OFF pathways in mouse retina. Eur. J. Neurosci. *36*, 2470–2481.

Madison, J.M., Nurrish, S., and Kaplan, J.M. (2005). UNC-13 interaction with syntaxin is required for synaptic transmission. Curr. Biol. *15*, 2236–2242.

Martin, J.A., Hu, Z., Fenz, K.M., Fernandez, J., and Dittman, J.S. (2011). Complexin has opposite effects on two modes of synaptic vesicle fusion. Curr. Biol. *21*, 97–105.

Maximov, A., Tang, J., Yang, X., Pang, Z.P., and Südhof, T.C. (2009). Complexin controls the force transfer from SNARE complexes to membranes in fusion. Science *323*, 516–521.

McEwen, J.M., Madison, J.M., Dybbs, M., and Kaplan, J.M. (2006). Antagonistic regulation of synaptic vesicle priming by Tomosyn and UNC-13. Neuron *51*, 303–315.

Miller, K.G., Alfonso, A., Nguyen, M., Crowell, J.A., Johnson, C.D., and Rand, J.B. (1996). A genetic selection for *Caenorhabditis elegans* synaptic transmission mutants. Proc. Natl. Acad. Sci. USA *93*, 12593–12598.

Mitchell, S.J., and Ryan, T.A. (2004). Syntaxin-1A is excluded from recycling synaptic vesicles at nerve terminals. J. Neurosci. *24*, 4884–4888.

Nonet, M.L., Saifee, O., Zhao, H., Rand, J.B., and Wei, L. (1998). Synaptic transmission deficits in *Caenorhabditis elegans* synaptobrevin mutants. J. Neurosci. *18*, 70–80.

Nurrish, S., Ségalat, L., and Kaplan, J.M. (1999). Serotonin inhibition of synaptic transmission: Galpha(0) decreases the abundance of UNC-13 at release sites. Neuron *24*, 231–242.

Prescott, E.D., and Zenisek, D. (2005). Recent progress towards understanding the synaptic ribbon. Curr. Opin. Neurobiol. *15*, 431–436.

Ramirez, F., and Jain, M.K. (1991). Phospholipase A2 at the bilayer interface. Proteins *9*, 229–239.

Ramot, D., Johnson, B.E., Berry, T.L., Jr., Carnell, L., and Goodman, M.B. (2008). The Parallel Worm Tracker: a platform for measuring average speed and drug-induced paralysis in nematodes. PLoS ONE *3*, e2208.

Reim, K., Wegmeyer, H., Brandstätter, J.H., Xue, M., Rosenmund, C., Dresbach, T., Hofmann, K., and Brose, N. (2005). Structurally and functionally unique complexins at retinal ribbon synapses. J. Cell Biol. *169*, 669–680.

Reim, K., Regus-Leidig, H., Ammermüller, J., El-Kordi, A., Radyushkin, K., Ehrenreich, H., Brandstätter, J.H., and Brose, N. (2009). Aberrant function

and structure of retinal ribbon synapses in the absence of complexin 3 and complexin 4. J. Cell Sci. *122*, 1352–1361.

Schaub, J.R., Lu, X., Doneske, B., Shin, Y.K., and McNew, J.A. (2006). Hemifusion arrest by complexin is relieved by Ca^{2+}-synaptotagmin I. Nat. Struct. Mol. Biol. *13*, 748–750.

Schlüter, O.M., Khvotchev, M., Jahn, R., and Südhof, T.C. (2002). Localization versus function of Rab3 proteins. Evidence for a common regulatory role in controlling fusion. J. Biol. Chem. *277*, 40919–40929.

Seiler, F., Malsam, J., Krause, J.M., and Söllner, T.H. (2009). A role of complexin-lipid interactions in membrane fusion. FEBS Lett. *583*, 2343–2348.

Strenzke, N., Chanda, S., Kopp-Scheinpflug, C., Khimich, D., Reim, K., Bulankina, A.V., Neef, A., Wolf, F., Brose, N., Xu-Friedman, M.A., and Moser, T. (2009). Complexin-I is required for high-fidelity transmission at the endbulb of Held auditory synapse. J. Neurosci. *29*, 7991–8004.

Südhof, T.C., and Rizo, J. (2011). Synaptic vesicle exocytosis. Cold Spring Harb. Perspect. Biol. *3*. http://dx.doi.org/10.1101/cshperspect.a005637.

Takamori, S., Holt, M., Stenius, K., Lemke, E.A., Grønborg, M., Riedel, D., Urlaub, H., Schenck, S., Brügger, B., Ringler, P., et al. (2006). Molecular anatomy of a trafficking organelle. Cell *127*, 831–846.

Walch-Solimena, C., Blasi, J., Edelmann, L., Chapman, E.R., von Mollard, G.F., and Jahn, R. (1995). The t-SNAREs syntaxin 1 and SNAP-25 are present on organelles that participate in synaptic vesicle recycling. J. Cell Biol. *128*, 637–645.

Wang, Z., Liu, H., Gu, Y., and Chapman, E.R. (2011). Reconstituted synaptotagmin I mediates vesicle docking, priming, and fusion. J. Cell Biol. *195*, 1159–1170.

Wichmann, C., and Sigrist, S.J. (2010). The active zone T-bar—a plasticity module? J. Neurogenet. *24*, 133–145.

Willumsen, B.M., Christensen, A., Hubbert, N.L., Papageorge, A.G., and Lowy, D.R. (1984). The p21 ras C-terminus is required for transformation and membrane association. Nature *310*, 583–586.

Xue, M., Reim, K., Chen, X., Chao, H.T., Deng, H., Rizo, J., Brose, N., and Rosenmund, C. (2007). Distinct domains of complexin I differentially regulate neurotransmitter release. Nat. Struct. Mol. Biol. *14*, 949–958.

Xue, M., Stradomska, A., Chen, H., Brose, N., Zhang, W., Rosenmund, C., and Reim, K. (2008). Complexins facilitate neurotransmitter release at excitatory and inhibitory synapses in mammalian central nervous system. Proc. Natl. Acad. Sci. USA *105*, 7875–7880.

Xue, M., Lin, Y.Q., Pan, H., Reim, K., Deng, H., Bellen, H.J., and Rosenmund, C. (2009). Tilting the balance between facilitatory and inhibitory functions of mammalian and Drosophila Complexins orchestrates synaptic vesicle exocytosis. Neuron *64*, 367–380.

Zhang, F.L., and Casey, P.J. (1996). Protein prenylation: molecular mechanisms and functional consequences. Annu. Rev. Biochem. *65*, 241–269.